Immunity
Article

Transmigrating Neutrophils Shape the Mucosal Microenvironment through Localized Oxygen Depletion to Influence Resolution of Inflammation

Eric L. Campbell,[1,*] Walter J. Bruyninckx,[2] Caleb J. Kelly,[1] Louise E. Glover,[1] Eóin N. McNamee,[1] Brittelle E. Bowers,[1] Amanda J. Bayless,[1] Melanie Scully,[1] Bejan J. Saeedi,[1] Lucy Golden-Mason,[3] Stefan F. Ehrentraut,[1] Valerie F. Curtis,[1] Adrianne Burgess,[1] John F. Garvey,[4] Amber Sorensen,[3] Raphael Nemenoff,[3] Paul Jedlicka,[3] Cormac T. Taylor,[4] Douglas J. Kominsky,[1] and Sean P. Colgan[1]

[1]Mucosal Inflammation Program, University of Colorado, Anschutz Medical Campus, Aurora, CO 80045, USA
[2]Department of Biology, Hanover College, Hanover, IN 47243, USA
[3]University of Colorado, Anschutz Medical Campus, Aurora, CO 80045, USA
[4]University College Dublin, Dublin 4, Ireland
*Correspondence: eric.campbell@ucdenver.edu
http://dx.doi.org/10.1016/j.immuni.2013.11.020

SUMMARY

Acute intestinal inflammation involves early accumulation of neutrophils (PMNs) followed by either resolution or progression to chronic inflammation. Based on recent evidence that mucosal metabolism influences disease outcomes, we hypothesized that transmigrating PMNs influence the transcriptional profile of the surrounding mucosa. Microarray studies revealed a cohort of hypoxia-responsive genes regulated by PMN-epithelial crosstalk. Transmigrating PMNs rapidly depleted microenvironmental O_2 sufficiently to stabilize intestinal epithelial cell hypoxia-inducible factor (HIF). By utilizing HIF reporter mice in an acute colitis model, we investigated the relative contribution of PMNs and the respiratory burst to "inflammatory hypoxia" in vivo. CGD mice, lacking a respiratory burst, developed accentuated colitis compared to control, with exaggerated PMN infiltration and diminished inflammatory hypoxia. Finally, pharmacological HIF stabilization within the mucosa protected CGD mice from severe colitis. In conclusion, transcriptional imprinting by infiltrating neutrophils modulates the host response to inflammation, via localized O_2 depletion, resulting in microenvironmental hypoxia and effective inflammatory resolution.

INTRODUCTION

Transmigration of neutrophils (PMNs, polymorphonuclear leukocytes) to regions of injury or infection is one of the earliest manifestations of acute inflammation, necessary for host defense. However, without efficient PMN clearance at sites of infiltration, PMNs can accumulate and contribute to chronic inflammatory states. Infiltration of PMNs is associated with a number of chronic disease states, including ischemic colitis, ulcerative colitis, and Crohn's disease. Energy-demanding processes such as migration, phagocytosis, and generation of an NADPH oxidase burst accompany infiltration of PMNs and are thought to shift the metabolic homeostasis of tissue during inflammation (Kominsky et al., 2010). Considerable advances in understanding the cell-cell interactions that facilitate PMN migration across epithelia have been made (Zen and Parkos, 2003). Relatively little is known, however, about the influence exerted by PMNs on surrounding cell types and whether such changes influence tissue function and disease outcome (Colgan et al., 2013a, 2013b).

In their role within innate immunity, PMNs detect and kill invading microbes, through mechanisms involving mobilization of plasma membranes and extrusion of granule contents (Stie and Jesaitis, 2007). Recruitment of PMNs to sites of infection results in killing of invading pathogens via release of granule contents (Amulic et al., 2012), phagocytosis with respiratory burst (Cross and Segal, 2004), release of reactive oxygen or nitrogen species (Radi et al., 1991), and in some instances generation of extracellular traps (Brinkmann et al., 2004). In this capacity, sites of inflammation tend to become depleted of molecular O_2 (Karhausen et al., 2004). These findings have led to the concept of "inflammatory hypoxia," in which inflammation and hypoxia are inextricably linked (Colgan and Taylor, 2010). It remains unclear to what extent inflammatory hypoxia impacts the local microenvironment and how such changes might influence disease outcome.

Here we demonstrate mechanisms and outcomes of inflammatory hypoxia in vitro and in vivo and implicate infiltrating immune cells, principally neutrophils, in shaping the tissue microenvironment through depletion of local molecular O_2. Guided by global mRNA profiling to ascertain whether PMNs "transcriptionally imprint" epithelial cells during transmigration in vitro, we hypothesized that PMN-dependent O_2 depletion is integral to regulating inflammatory resolution. Microarray analysis revealed a cohort of hypoxia-responsive genes. Validation studies demonstrated that activated PMNs are capable of depleting local O_2 to such an extent that epithelia in close proximity "sense" hypoxia and stabilize the HIF transcriptional machinery. This influence on epithelial HIF activity was dependent on the PMN respiratory burst. Moreover, such localized

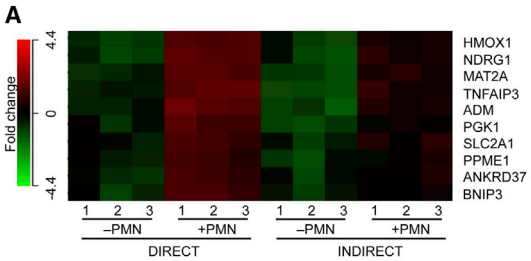

B

	Direct –PMN Vs +PMN		Indirect –PMN Vs +PMN	
Gene	Regulation	Fold	Regulation	Fold
HMOX1	Up	1.51	Up	3.99
NDRG1	Up	2.03	Up	1.81
SLC2A1(Glut1)	Up	3.54	Up	4.31
MAT2A	Up	1.57	Up	2.71
ADM	Up	1.81	Up	3.96
PGK1	Up	1.44	Up	1.70
PPME1	Up	2.63	Up	4.52
BNIP3	Up	2.26	Down	1.19
ANKRD37	Up	2.50	Up	5.32

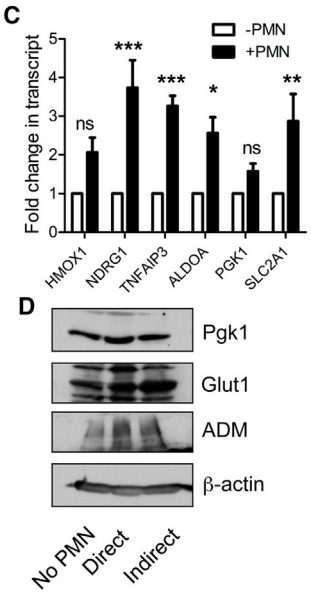

Figure 1. Transmigrating Neutrophils Induce Transcriptional Imprinting in Intestinal Epithelial Cells

(A) Microarrays were hybridized with cDNA synthesized from epithelial RNA isolated from direct versus indirect transmigration experiments. Three separate experiments were performed (n = 3).

(B) Table highlighting fold changes between groups. Statistical cut-off was set to $p < 0.05$.

(C) Validation of hypoxia-responsive gene cluster by qPCR in the indirect model. Values are means ± SEM and are pooled from three independent experiments (n = 3; *$p < 0.05$; **$p < 0.01$; ***$p < 0.001$; two-way ANOVA).

(D) Validation of hypoxia-responsive target induction by immunoblotting for GLUT1, PGK1, and ADM. β-actin used as loading control. Images are representative of three independent experiments.

See also Figure S1.

O_2 depletion proved to be critical for effective mucosal protection and inflammatory resolution.

RESULTS

Neutrophil Transepithelial Migration Induces Expression of Hypoxia-Dependent Genes

To define the impact of PMN transmigration on the transcriptional profile of intestinal epithelial cells (IECs), we induced PMNs to migrate across IECs, harvested RNA, and analyzed transcriptional profiles by microarray. Pilot studies involving magnetic bead negative selection involved excessive manipulation and time and resulted in widespread cell death. To minimize alterations in the transcriptional profile as a result of handling, we adopted a different approach to rapidly obtain representative mRNA. Parallel experiments were performed. First, PMNs were induced to transmigrate toward fMLF across polarized monolayers of IECs for 90 min, monolayers were washed in fresh medium, and after 2 hr RNA was harvested (Figure S1A available online). Because of the physical interaction of PMN-IECs, we termed this "direct" migration. In the second experiment, migration toward fMLF was performed as before, cell-free supernatants were collected after transmigration and applied to naive IEC monolayers (Figure S1B), and after 2 hr RNA was harvested. This model was termed "indirect" because of the lack of physical contact between harvested IECs and PMNs. In the direct experiment, profiling revealed predominantly PMN-specific genes, because of contamination of the monolayer with incompletely migrated neutrophils. In the indirect experiment, gene regulation induced by physical contact between neutrophils and epithelial cells were lost. However, genes regulated as a result of factors released during transmigration were present. Analyzing genes that were similarly regulated in both experiments enabled us to discern epithelial-specific regulation of genes in response to activated PMNs (Figure 1A). We identified a cohort of hypoxia-regulated genes that were induced in both models in response to PMNs (Figure 1B). Gene targets from hypoxia-responsive cluster were validated by qPCR via cDNA from indirect transmigration (Figure 1C) and by immunoblot (Figure 1D) by means of lysates from both direct and indirect for GLUT1, PGK1, and ADM.

Activated Neutrophils Imprint a Hypoxic Microenvironment into the Surrounding Tissue

Guided by our findings that PMN transmigration establishes a hypoxic niche, we developed a system to allow for real-time O_2 monitoring. Initial experiments were performed with an Oxylite 2000 probe. Neutrophils were incubated in a hypoxia chamber set at 4% O_2 in the presence of the chemotactic peptide fMLF (N-formyl-methionine-leucine-phenylalanine). A time-dependent depletion of dissolved O_2 was observed (Figure 2A). Given the need for more high-throughput analysis, we adapted a real-time O_2 sensor (SDR, PreSens) where PMNs were suspended above the sensor (Figure S1D), which promptly depleted all dissolved O_2. With this system we demonstrated that activated PMNs rapidly deplete all available O_2 in a cell number- and chemoattractant-dependent manner (Figure 2B).

We sought to ascertain whether PMN-mediated O_2 depletion was sufficient for epithelial cells in close proximity to "sense" hypoxia. PMNs were suspended in a 0.4 μm pore Transwell above T84 intestinal epithelial cells (Figure S1C) in the presence of hypoxia-dependent adduct-forming compound (pimonidazole-HCl) dye and activated with fMLF. After 0 min (Figure 2C) and 60 min (Figure 2D), cells were fixed and localized for hypoxia adducts with Hypoxyprobe-1 antibody. In parallel, examination of epithelial nuclear extracts revealed that PMN transmigration readily stabilized HIF at 3 and 6 hr of exposure (Figure 2E). To ascertain whether increased nuclear HIF levels resulted in transcriptional activity, HRE-luciferase reporter assays were employed and revealed that incubation of transfected IECs with activated PMNs for 3 or 6 hr resulted in increased HIF activity as reflected by increased luciferase signal (Figure 2F).

Next we examined the mechanism of O_2 depletion by PMNs. Neutrophils were exposed to either vehicle (DMSO) or

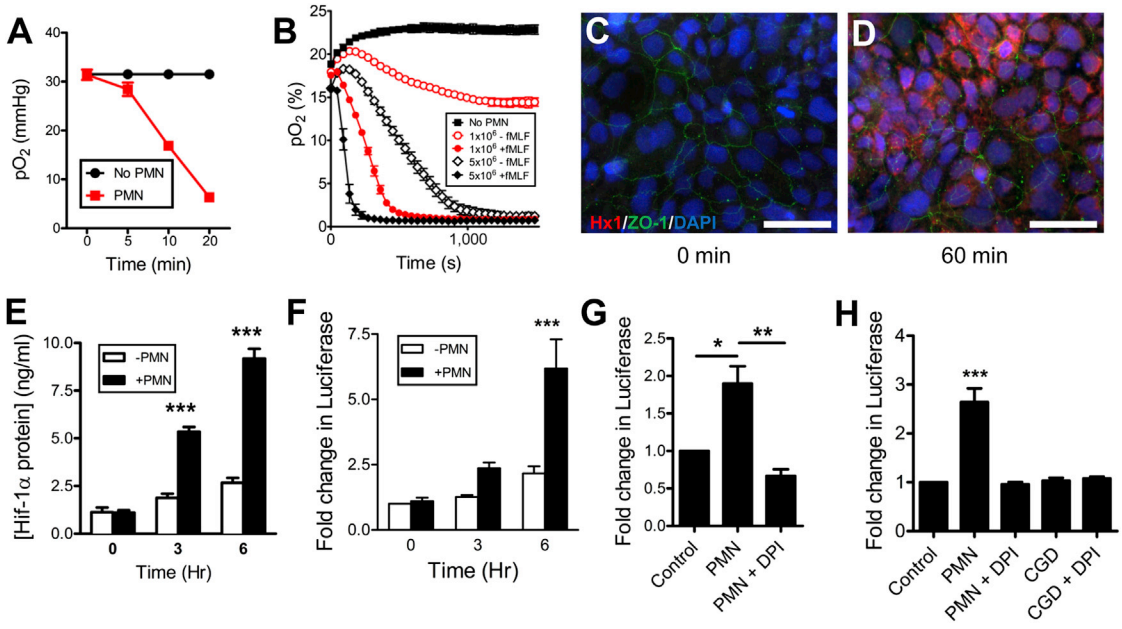

Figure 2. Activated Neutrophils Rapidly Deplete O_2 and Induce HIF-1α Stabilization via Respiratory Burst

(A) pO_2 values were recorded in hypoxia chamber set to 4% O_2, by means of a OxoProbe at indicated time points in the presence of 1 × 10^6 PMNs, activated with fMLF. Data are representative of three independent experiments and presented as means ± SD (n = 3; $p < 0.001$; two-way ANOVA).

(B) Consumption of dissolved O_2 in normoxia was monitored in real-time by OxoDishes mounted on an SDR O_2 sensor reader in the presence of increasing numbers of PMN ± activation with fMLF set up with the SDR real-time O_2 (see Figure S1D) model. Data are representative of three independent experiments and presented as means ± SD (n = 3; $p < 0.001$ throughout time course for ±PMN; $p < 0.001$ throughout time course for 1 × 10^6 PMNs ± chemoattractant; $p < 0.001$ between 46 and 948 s for 5 × 10^6 PMN ± chemoattractant; $p < 0.001$ between 46 and 407 s for 1 × 10^6 versus 5 × 10^6 with chemoattractant; two-way ANOVA).

(C and D) Immunofluorescent staining of T84 IECs exposed to PMNs by the coculture model (see Figure S1C) for 0 min (C) and 60 min (D); representative images from two independent experiments. Hypoxyprobe-1 adduct staining (red), ZO-1 (green), and nuclei (blue). Scale bars represent 200 μm.

(E) Nuclear accumulation of HIF-1α protein was assayed by Mesoscale ELISA, after exposure of epithelia to activated PMNs by coculture model. Data are represented as means ± SEM and are pooled from three independent experiments (n = 3; $p < 0.001$ by two-way ANOVA).

(F) IECs transfected with HRE-firefly and SV40-renilla Luciferase reporters and subsequently exposed to activated PMNs indicated increased HIF activity. Data are represented as means ± SEM and are pooled from three independent experiments (n = 3; $p < 0.001$ by two-way ANOVA).

(G) IECs transfected with HRE-firefly and SV40-renilla luciferase reporters and subsequently exposed to pretreated PMNs in the presence of fMLF. Data are represented as means ± SEM and are pooled from three independent experiments (n = 3; $p < 0.05$ for ±PMN; $p < 0.01$ for PMN versus PMN+DPI; one-way ANOVA; DPI = diphenyleneiodonium).

(H) HRE-transfected Caco-2 IECs, with subsequent exposure to activated PMNs from wild-type or CGD mice. Data are represented as means ± SEM and are pooled from three independent experiments (n = 3; $p < 0.001$ for no PMN versus wild-type PMN; $p > 0.05$ for no PMN versus PMN+DPI; $p > 0.05$ for no PMN versus CGD PMN; one-way ANOVA).

See also Figure S2.

diphenyleneiodonium (DPI, to inhibit the respiratory burst) (Cross and Jones, 1986) for 15 min, washed in PBS, and exposed to HRE-Luc-transfected IECs. PMNs without pretreatment resulted in an induction of luciferase whereas DPI completely abrogated PMN-mediated stabilization of HIF in adjacent IECs (Figure 2G). These findings strongly implicate the PMN respiratory burst in microenvironmental depletion of molecular O_2.

Mice lacking functional NADPH oxidase in PMNs (*Nox2*$^{-/-}$, or CGD mice) phenotypically mirror human chronic granulomatous disease (CGD) because of a deficiency in PMN respiratory burst activity (Dinauer et al., 1987). To define the contribution of the respiratory burst in O_2 depletion, we harvested bone marrow PMNs from both wild-type C57BL/6 and CGD mice, incubated with/without DPI for 15 min on ice, and tracked consumption of dissolved O_2 by utilizing a novel real-time O_2 sensor (Figure S2). As proof-of-principle, PMNs from phorbol myristate acetate (PMA)-activated wild-type mice increased luciferase activity in HRE-transfected epithelia, and this influence was abrogated with DPI. Moreover, CGD PMNs were incapable of inducing epithelial hypoxia (Figure 2H) in the presence or absence of DPI. Taken together, these data demonstrate that PMNs deplete sufficient O_2 to render nearby IECs hypoxic, via the NADPH oxidase burst.

Neutrophil Infiltration Establishes a Hypoxic Microenvironment during Acute Colonic Inflammation

To recapitulate our findings in vivo, we utilized the trinitrobenzenesulfonic acid (TNBS) colitis model of murine acute colonic inflammation. Chemically induced models of colitis are frequently criticized for not accurately recapitulating ulcerative colitis in humans, a chronic inflammatory condition complicated by defects of both innate and adaptive immunity (Khor et al., 2011), and are considered merely models of acute colonic inflammation. We elected to use TNBS over other acute models of colonic inflammation because of its early potent recruitment of PMNs (maximal at 12–24 hr). The dextran sulfate sodium model,

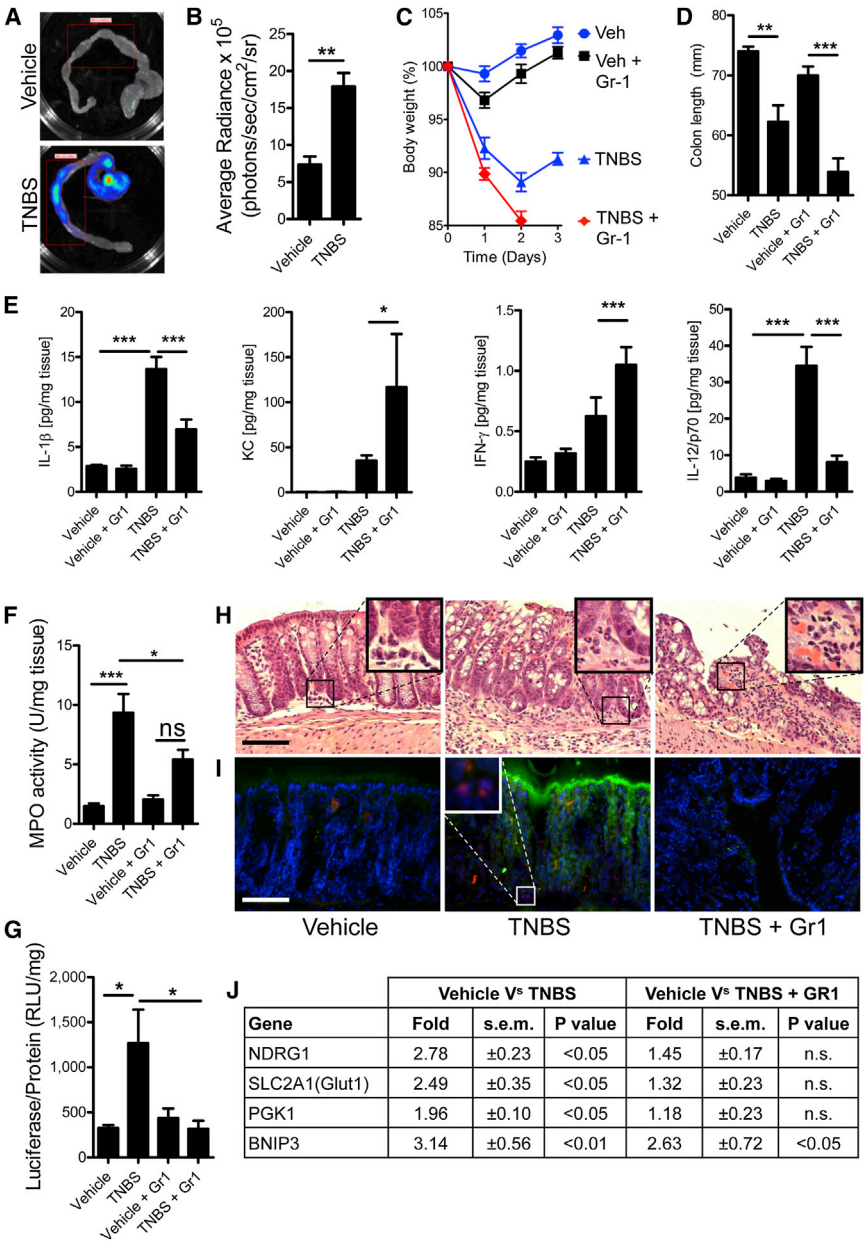

J

	Vehicle Vs TNBS			Vehicle Vs TNBS + GR1		
Gene	Fold	s.e.m.	P value	Fold	s.e.m.	P value
NDRG1	2.78	±0.23	<0.05	1.45	±0.17	n.s.
SLC2A1(Glut1)	2.49	±0.35	<0.05	1.32	±0.23	n.s.
PGK1	1.96	±0.10	<0.05	1.18	±0.23	n.s.
BNIP3	3.14	±0.56	<0.01	2.63	±0.72	<0.05

Figure 3. Neutrophil Accumulation in Colitis Induces Inflammatory Hypoxia

(A) Representative image of colons excised from vehicle and TNBS-treated ODD-Luc reporter mice, injected with D-Luciferin before sacrifice and imaged for luciferase activity.

(B) Quantification of bioluminescent imaging values represent mean ± SEM (n = 5; **p < 0.01; two-tailed Student's t test).

(C and D) Gr-1 antibody was used to deplete PMNs in ODD-Luc mice, prior to induction of colitis with TNBS. PMN-depleted ODD-Luc mice developed more severe colitis than did sham injected mice, demonstrated by (C) weight-loss curves ($p < 0.001$ for vehicle versus TNBS; $p < 0.001$ TNBS versus TNBS+Gr-1; two-way ANOVA) and (D) colon length ($p > 0.05$ for vehicle versus TNBS; $p < 0.05$ for vehicle+Gr-1 versus TNBS+Gr-1; one-way ANOVA). Data are represented as means ± SEM and are pooled from three independent experiments (n = 12).

(E) Protein lysates were profiled for cytokines and normalized to total protein (*p < 0.05; ***p < 0.001; one-way ANOVA).

(F) MPO activity in tissues after TNBS ± Gr-1. Data are represented as means ± SEM and are pooled from three independent experiments (n = 12).

(G) Tissue homogenates from distal colons of TNBS-treated mice ± Gr-1 depletion revealed an increase in luciferase activity in TNBS-treated mice ($p < 0.05$) that was attenuated by Gr-1 depletion ($p < 0.05$; one-way ANOVA). Data represented as means ± SEM and pooled from two independent experiments (n = 8).

(H) Representative H&E-stained sections revealed PMN accumulation in TNBS, which was attenuated by Gr-1. Inset highlights typical infiltrate observed.

(I) IHC for luciferase and Ly6g indicated accumulation of PMNs in TNBS (highlighted in inset), which coincided with hypoxic luciferase accumulation and an abrogation of both with Gr-1 depletion. Scale bars represent 100 μm.

(J) Fold increases in HIF target gene transcript expression in TNBS ± Gr-1 measured by qPCR, data represent means ± SEM and are pooled from three independent experiments (n = 12).

See also Figure S3.

which relies on denuding epithelia to expose the mucosa to luminal contents, makes investigation of PMN-epithelial interactions difficult. Finally, TNBS is a self-resolving acute inflammation, making it an ideal model to study PMN-epithelial interactions in the context of colonic inflammation (Van Rees et al., 1997). By utilizing HIF reporter ODD-luc mice (Safran et al., 2006) in combination with whole-tissue imaging, we quantified induction of colonic inflammation-associated hypoxia (Figures 3A and 3B). Maximal luciferase expression in colitis was observed in the cecum (Figure 3A) and was patchy throughout the colon of colitic animals.

To define the role of PMNs in tissue hypoxia during colitis, we depleted PMNs by using Gr-1 in ODD-luc mice (Kühl et al., 2007) and elected to harvest after 2 days to capture tissue changes occurring before clearance of PMNs by macrophages. Flow cytometry indicated a >90% depletion of circulating PMNs with Gr-1 (91.63% in vehicle and 97.47% in TNBS), with minimal influence on circulating monocyte numbers (Figure S3). TNBS administration resulted in marked weight loss on days 1 and 2 (Figure 3C). Depletion of PMNs during colitis resulted in ultimately more severe weight loss on day 2 (Figure 3C). A trend toward colon shortening occurred with TNBS, but with PMN depletion, greater colon shortening was observed (Figure 3D). Tissue myeloperoxidase (MPO) measurements were performed to quantify PMN influx and demonstrated a reduced number of tissue PMNs during colitis (Figure 3E). Multiplex ELISAs revealed increases of tissue cytokines for IL-1β and IL-12/p70 in TNBS, which was abrogated by Gr-1 depletion of PMNs. Additionally, increases in tissue IFN-γ and mKC were observed in TNBS but levels were amplified by PMN depletion (Figure 3F). Tissue

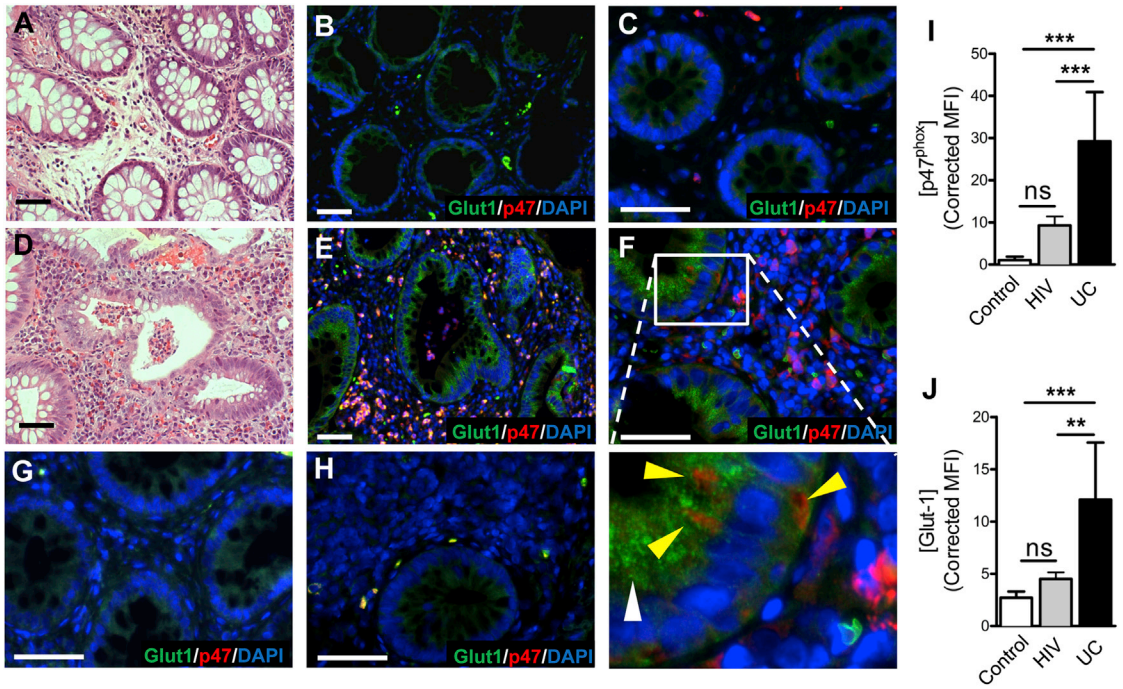

Figure 4. Ulcerative Colitis Patients with Crypt Abscesses Demonstrate Hypoxia-Dependent Target Induction

(A–F) Biopsies from (A, B, C) uninflamed margins and (D, E, F) inflamed regions with active crypt abscess formation in patients with ulcerative colitis, were processed for H&E (A, D) and stained for hypoxia-responsive Glut-1 (green), neutrophil $p47^{phox}$ (red), and nuclei (blue). Higher magnification of uninflamed tissue (C) or colitis (F) indicates de novo Glut1 (white arrowhead) adjacent to transmigrating PMN (yellow arrowhead).

(G and H) Disease controls from uninflamed (G) and HIV patient (H) biopsies.

(I and J) Quantification of staining intensities for p47 (I) and Glut1 (J). Measurements were made from five ROIs per slide and five slides per group. Data represent means ± SEM (n = 25). (**$p < 0.01$; ***$p < 0.001$; one-way ANOVA).

Scale bars represent 50 μm.

HIF-dependent luciferase activity was abrogated by Gr-1-mediated PMN depletion (Figure 3G). Histologic examination revealed a prominent granulocytic infiltrate in TNBS mice coupled with severe mucosal damage (Figure 3H, middle), consistent with clinical parameters of weight loss and colon shortening (Figures 3C and 3D). PMN depletion aggravated the mucosal damage, wherein infiltrating leukocytes were non-PMN cell types (Figure 3H, right), consistent with previous findings that PMN depletion significantly enhances inflammation in colitis in rats (Kühl et al., 2007). Immunohistochemical staining for hypoxia-dependent firefly luciferase (green) and neutrophil-specific marker Ly6g (red) indicated a concomitant induction of luciferase in regions of neutrophil infiltration in TNBS (Figure 3I, middle) relative to vehicle-treated mice (Figure 3I, left) or in TNBS with Gr-1-mediated PMN depletion (Figure 3I, right). Finally, isolated epithelia were assessed for changes in mRNA (Figure 3J), demonstrating an overall decrease in hypoxic target gene expression with Gr-1. Taken together, such findings substantiate our in vitro results that infiltrating PMNs deplete local O_2 amounts and that ensuing hypoxia influences the severity of the inflammatory response.

Evidence of Microenvironmental Hypoxia in Crypt Abscesses

We extended these findings to humans and identified biopsies from patients with ulcerative colitis that showed active disease with crypt abscess formation. Serial sections were stained for H&E and immunohistochemical detection of the HIF target Glut1. As shown in Figure 4, tissue margins revealed healthy crypts (Figure 4A) and low expression of Glut1 (Figure 4B). In stark contrast, regions of tissue with active crypt abscesses (Figure 4D) revealed prominent parallel localization of PMNs and robust staining for Glut1 (Figure 4E). Higher magnification of control (Figure 4C) and colitis (Figure 4F) revealed de novo staining surrounding transmigrating PMNs (inset, Figure 4F). Colonic biopsies from uninflamed patients (Figure 4G) and HIV patients (Figure 4H) with marked T cell infiltration but few neutrophils were stained as an inflammatory disease control to demonstrate specificity of tissue hypoxic responses to PMNs. Quantification of image intensities illustrates PMN (Figure 4I) and Glut1 (Figure 4J) staining. Thus, inflammatory hypoxia occurs in vivo and is specific for inflammatory lesions associated with PMN influx.

Mice Lacking Respiratory Burst Exhibit Defective Inflammatory Resolution

To specifically delineate the influence of the PMN respiratory burst in the establishment of a hypoxic microenvironment during colitis, we attempted to induce colitis in the CGD mice. In these mice, TNBS elicited a response so prominent that few animals survived (Figure 5A). A dose response with various concentrations of TNBS and vehicle carrier (ethanol) identified conditions that permitted the study of colitis without excessive attrition

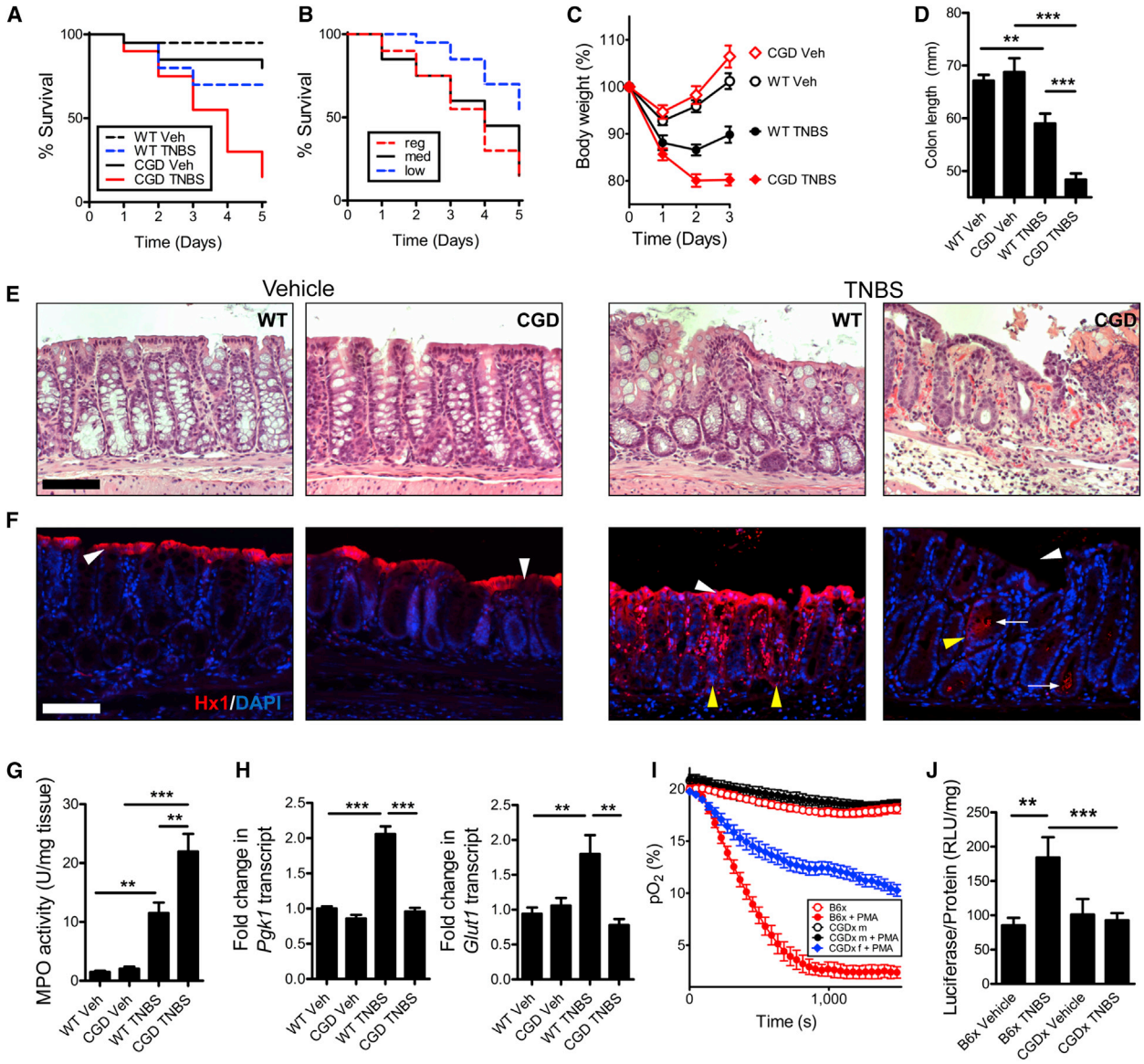

Figure 5. Neutrophil Respiratory Burst-Deficient Mice Develop Severe Nonresolving Colitis

(A) Survival curves for C57BL/6 versus CGD mice after TNBS administration ($p < 0.001$ compared with vehicle; $p < 0.05$ compared with wild-type TNBS; Gehan-Breslow-Wilcoxon test). Data represent means ± SEM (n = 6).

(B) Survival curves for CGD mice on regular (reg) (2.5% TNBS in 50% EtOH), medium (med) (2% TNBS in 45% EtOH), and low (low) (2% TNBS in 40% EtOH) TNBS regimen. Data represent means ± SEM (n = 6) ($p < 0.005$ low compared with regular dose; $p < 0.05$ low compared with medium dose TNBS; Gehan-Breslow-Wilcoxon test).

(C and D) Weight-loss curves (C) and colon lengths (D) of CGD mice on low TNBS regimen indicated a defect in resolution. Data are represented as means ± SEM and are pooled from three independent experiments (n = 8–12).

(E) Representative H&E-stained sections revealed severe PMN accumulation in CGD mice treated with TNBS.

(F) Hypoxyprobe (red) staining and nuclear (blue) counterstain of wild-type versus CGD mice ± TNBS. White arrowheads indicate presence or absence of luminal epithelial cells; yellow arrowheads indicate crypts. Arrows indicate potential presence of bacteria.

Scale bars represent 100 μm.

(G) Myeloperoxidase activity assay indicated increased PMNs in TNBS (**$p < 0.01$; ***$p < 0.001$; one-way ANOVA). Data are represented as means ± SEM and are pooled from three independent experiments (n = 8–12).

(H) Hypoxia target gene expression from purified colonic epithelial cells for *Pgk1* and *Glut1* in TNBS. Data are represented as means ± SEM (**$p < 0.01$; ***$p <$ 0001; one-way ANOVA).

(I) O_2 consumption of B6x versus CGDx m (male) and f (female) ($p < 0.001$ B6x ± PMA; $p > 0.05$ male CGDx ± PMA; $p < 0.001$ female CGDx versus B6x –PMA; $p <$ 0.001 female CGDx versus B6x +PMA; two-way ANOVA). Data are representative of three independent experiments and presented as means ± SD (n = 6).

(J) Tissue luciferase was assayed after a low TNBS regimen in both B6x ($p < 0.01$ vehicle versus TNBS in B6x) and CGDx ($p > 0.05$ CGDx vehicle versus TNBS; $p <$ 0.05 for B6x TNBS versus CGDx TNBS; one-way ANOVA). Data are represented as means ± SEM and are pooled from two independent experiments (n = 8).

See also Figure S4.

(Figure 5B). In wild-type mice, peak disease usually occurs on day 2, with resolution beginning on day 3. Based on weight loss curves (Figure 5C) and colon length (Figure 5D), the lack of a respiratory burst appeared to impede the resolution phase of disease. Such findings were not a result of failure of PMNs to migrate to the tissue, evidenced by myeloperoxidase activity (Figure 5G). Indeed, histologic examination of these tissues revealed prominent increase in PMNs within the colonic submucosa of CGD mice (Figure 5E), which may indicate delayed or failed resolution. In Figure 5F, sections were stained with Hypoxyprobe-1. Vehicle-treated wild-type and CGD mice displayed prominent luminal epithelial staining, indicated by white arrowheads. TNBS resulted in extensive Hypoxyprobe-1 staining, permeating deep into the crypt structure, indicated by yellow arrowheads. Concomitant with increased PMN infiltration, the CGD mice had an appreciable lack of Hypoxyprobe-1 staining within the mucosa. Most striking was the apparent lack of luminal epithelial staining. Notable were regions with what appear to be bacteria deep in crypt lumen, wherein the epithelium responded with positive Hypoxyprobe-1 staining (white arrows). Enrichment of epithelial cells followed by RNA isolation and qPCR revealed increased expression of *Pgk1* and *Glut1* transcripts in TNBS-treated wild-type, which were not induced in CGD mice (Figure 5H).

To quantify the relative contribution of the respiratory burst to hypoxia in colitis, we bred a first-generation cross of CGD mice with the ODD-luc mice (CGDx) and a control C57BL/6 crossed to ODD-luc (B6x) (see Figure S4 for breeding strategy). Because *Nox2* is X-linked, mating female CGD mice with ODD-luc males resulted in a progeny that was either hemizygous for the CGD phenotype (females) or homozygous (males). Bone-marrow-derived PMNs from the control cross (B6x) consumed O_2 rapidly in response to PMA stimulation; however, male CGDx mice did not deplete O_2 in response to activation. Hemizygous female CGDx mice did deplete O_2, but at a slower rate than the B6x mice (Figure 5I). Moreover, tissue luciferase levels from B6x mice reaffirm the finding that TNBS induces tissue hypoxia (Figure 5J) because male CGDx mice were unable to generate a hypoxic microenvironment in response to TNBS, as measured by tissue luciferase (Figure 5J). These findings demonstrate that CGD mice develop severe nonresolving colonic inflammation coupled with a failure to elicit mucosal hypoxia.

Mucosal HIF Stabilization Ameliorates Colitis Severity in Mice Lacking Respiratory Burst

Our previous work demonstrated that pharmacological HIF stabilization is protective in mucosal inflammation in wild-type mice (Robinson et al., 2008). We consequently proposed that the severity of colitis in CGD mice was due to a lack of hypoxic signaling within the mucosa. We examined whether pharmacological intervention could restore normal hypoxic signaling, recapitulate the wild-type inflammatory hypoxic microenvironment within the mucosa, and attenuate the severity of colitis in the CGD mice. To accomplish in vivo HIF stabilization, both wild-type and CGD mice were administered the PHD inhibitor (HIF stabilizer) AKB-4924 (Okumura et al., 2012). In wild-type mice, TNBS administration with sham injection resulted in weight loss (Figure 6A, top; $p < 0.001$ compared with vehicle on days 1–4 by two-way ANOVA). AKB-4924 administration was protective as reflected by decreased weight loss ($p < 0.001$ compared with TNBS alone on days 2–4; $p > 0.05$ compared with vehicle + AKB-4924 on days 2–3) and a more rapid return to normal body weight. In the CGD mice, TNBS elicited severe weight loss (Figure 6A, bottom; $p < 0.001$ compared with CGD vehicle on days 1–4). By day 3, TNBS-treated wild-type mice regained weight, which was not evident in CGD mice ($p < 0.05$ CGD versus WT + TNBS on day 3). Although an improvement was observed in the CGD mice with AKB-4924 administration ($p < 0.05$ on day 1; $p < 0.01$ on day 2; $p < 0.001$ on day 3–4), there remained a significant difference between the vehicle-treated and the AKB-4924-treated CGD mice ($p < 0.001$). In fact, AKB-4924 administration during colitis to CGD mice more closely resembled wild-type mice with TNBS ($p > 0.05$ by two-way ANOVA).

AKB-4924 administration resulted in protection against colon shortening in both wild-type and CGD mice (Figures S5A and S5B). Histological scoring revealed increases in both inflammatory score and injury score of wild-type and CGD mice after TNBS administration (Figure 6B). Although no significant differences were observed in the overall inflammatory score between wild-type and CGD-TNBS treatments without AKB-4924, CGD mice exposed to TNBS without AKB-4924 demonstrated higher injury scores. Moreover, AKB-4924 attenuated both inflammatory and injury scores. These findings were also evident by H&E (Figure 6E, top; see also Figure S6A).

Colon tissues were processed for flow cytometry to determine the extent of infiltration of various cell types. TNBS resulted in increased recruitment of $CD45^+$ cells to the colon in both wild-type and CGD mice. Interestingly, in CGD mice, the increase in $CD45^+$ cells appeared to be predominantly neutrophils and monocytes, both of which were abrogated by AKB-4924 administration (Figure 6C, see also Figure S5C). No appreciable differences in total $CD3^+$ T cell numbers were observed.

Tissue cytokines were assayed and revealed trends toward increased proinflammatory cytokines (IL-1β, IFN-γ, mKC, and IL-12) in both wild-type and CGD mice during TNBS that were largely abrogated by AKB-4924. Furthermore, mucosal protective cytokine (IL-6 and IL-10) levels were enhanced by HIF stabilization (Figure 6D). Considering the role of bioactive lipids in resolution of acute inflammation (Serhan and Chiang, 2013) and our previous findings demonstrating resolution of colitis with proresolving lipids (Campbell et al., 2010), we assessed the influence of TNBS and AKB-4924 treatment on the generation of proresolving lipids, including Resolvin D1 (RvD1) and 15-epi-Lipoxin A4 (Figure S5D). Tissue ELISAs revealed increased local RvD1 generation (after TNBS treatment) in wild-type and a decrease in CGD mice. Significant increases in RvD1 were observed after AKB-4924 treatment in both wild-type ($p < 0.001$) and CGD ($p < 0.05$) mice. Similarly, trends toward increased 15-epi-LXA4 were detected in TNBS-treated wild-type mice and decreased levels in CGD. A significant increase was detected in wild-type mice after treatment with the PHD inhibitor ($p < 0.05$). To rationalize these findings, we investigated expression of *Ptgs2* (cyclooxygenase-2), an enzyme involved in the de novo generation of both of these lipids and a known hypoxia-dependent gene. We detected a trend toward increased *Ptgs2* transcript in wild-type mice after TNBS treatment and in AKB-4924-treated colitic mice (Figure S5E) and increases in expression in CGD after PHD inhibition.

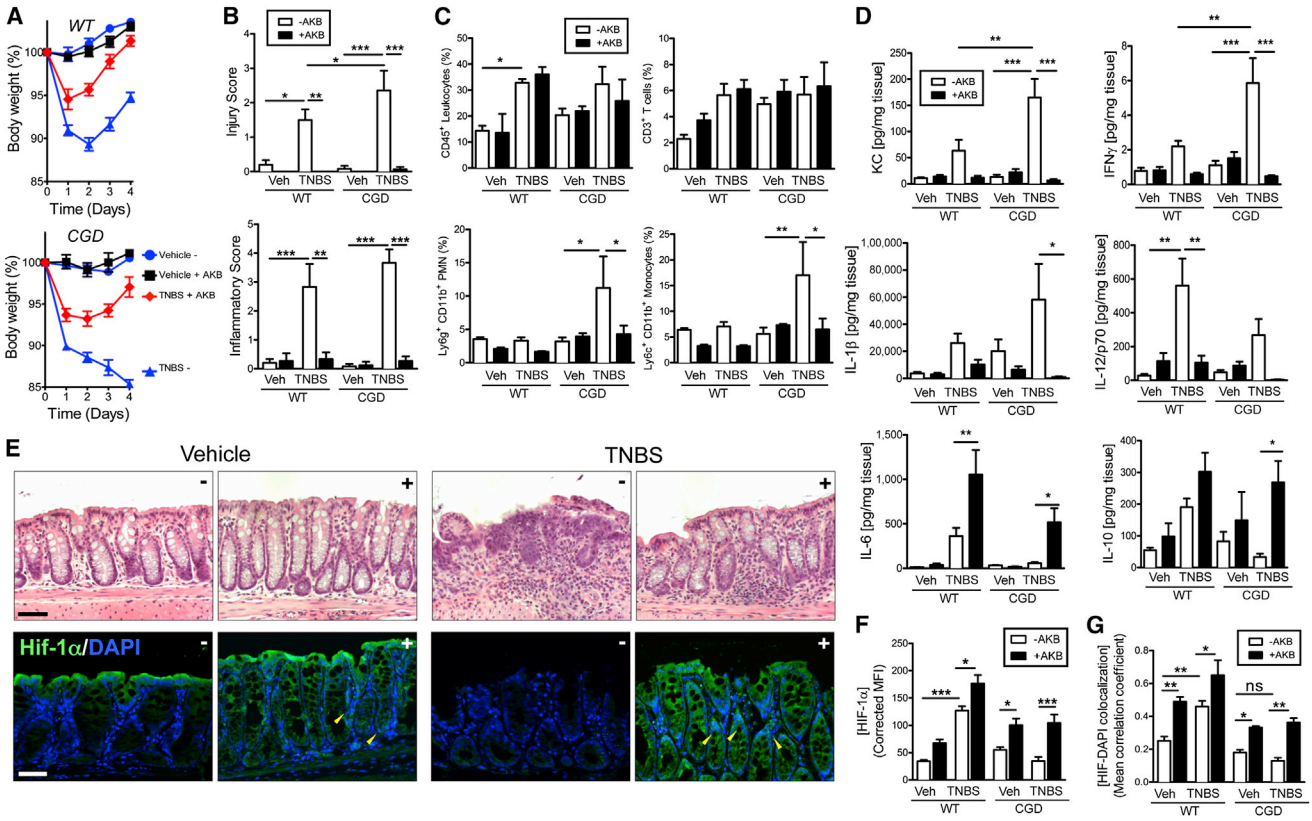

Figure 6. Pharmacological Intervention with Prolyl Hydroxylase Inhibitor Rectifies Resolution Defect in CGD Mice

Wild-type and CGD mice treated with AKB-4924 or vehicle on days −1 through 2 and TNBS or vehicle was administered on day 0.

(A) Weight loss curves for wild-type ($p < 0.001$ for vehicle versus TNBS on days 1–3; $p < 0.001$ TNBS versus TNBS+ AKB-4924 on days 2–3; $p > 0.05$ TNBS+AKB-4924 versus vehicle+ AKB-4924 on days 2–3) and CGD ($p < 0.001$ CGD vehicle versus CGD TNBS on days 1–3; two-way ANOVA) mice. Data are represented as means ± SEM and are pooled from three independent experiments (n = 8–12).

(B) Histological scoring of colon sections (n = 4–6; *$p < 0.05$; **$p < 0.01$; ***$p < 0.001$; one-way ANOVA).

(C) Flow cytometric analysis of infiltrating leukocytes: $CD45^+$ (bulk leukocytes), $CD3^+$ (T cells), $Ly6g^+CD11b^+$ (neutrophils), and $Ly6c^+CD11b^+$ (monocytes) (*$p < 0.05$; **$p < 0.01$; two-way ANOVA). Data are representative of two independent experiments and presented as means ± SD (n = 4–6 mice per group) ($p < 0.01$ by one-way ANOVA).

(D) Tissue ELISAs for cytokines from wild-type and CGD mice treated with AKB-4924 ± TNBS (*$p < 0.05$; **$p < 0.01$; ***$p < 0.001$; one-way ANOVA). Data are represented as means ± SEM and are pooled from three independent experiments (n = 8–12).

(E) Representative H&E-stained sections (top) from CGD mice with (+) or without (−) AKB-4924 and IHC staining (bottom) for HIF-1α (green) and nuclei (blue). Scale bars represent 100 μm. Yellow arrowheads indicate colocalization in TNBS and AKB-4924-treated crypt epithelial cells.

(F and G) Quantification of staining intensities (F) for HIF-1α and colocalization analysis (G) of HIF-1α with nuclear DAPI. Data are represented as means ± SEM of three pooled experiments (n = 8–12) (*$p < 0.05$; **$p < 0.01$; ***$p < 0.001$; one-way ANOVA).

See also Figures S5 and S6.

Immunohistochemical staining for Hypoxyprobe-1 (Figure S6B) indicated enhanced tissue hypoxia in wild-type mice after TNBS administration, but this was absent in CGD mice. These disparate phenotypes were both abrogated by AKB-4924 treatment. Sections were also stained for HIF-1α in CGD (Figure 6E, bottom) and wild-type (Figure S6C), which revealed both enhanced HIF-1α staining (Figure 6F) and colocalization of HIF-1α with nuclei in colonic crypts after AKB-4924 administration (indicated by yellow arrowheads and quantified in Figure 6G), demonstrating that AKB-4924 mediated HIF-1α stabilization within the mucosa. Taken together, these studies reveal that the innate immune deficit of CGD mice can be overcome by PHD inhibition within the colonic mucosa.

Mucosal HIF Stabilization Enhances Barrier Function by Increasing Goblet Cell Number

We elected to focus on the apparent infiltration of bacteria in the colonic crypts of CGD mice during colitis by utilizing fluorescent in situ hybridization (FISH) with a ubiquitous Eubacterial probe. In both CGD (Figure 7A) and wild-type (Figure S7A) vehicle-treated mice, bacteria associate with luminal epithelia. There was no indication of bacterial invasion into the mucosa. Upon exposure to TNBS, bacteria were observed to invade deep into the crypts of CGD but not wild-type mice (Figure S7A). Conversely, in PHD-inhibited mice, bacteria were not observed to interact with epithelia and a clear margin was observed. To determine whether these bacteria disseminate past the mucosa, we aseptically removed mesenteric lymph nodes (MLNs) and harvested

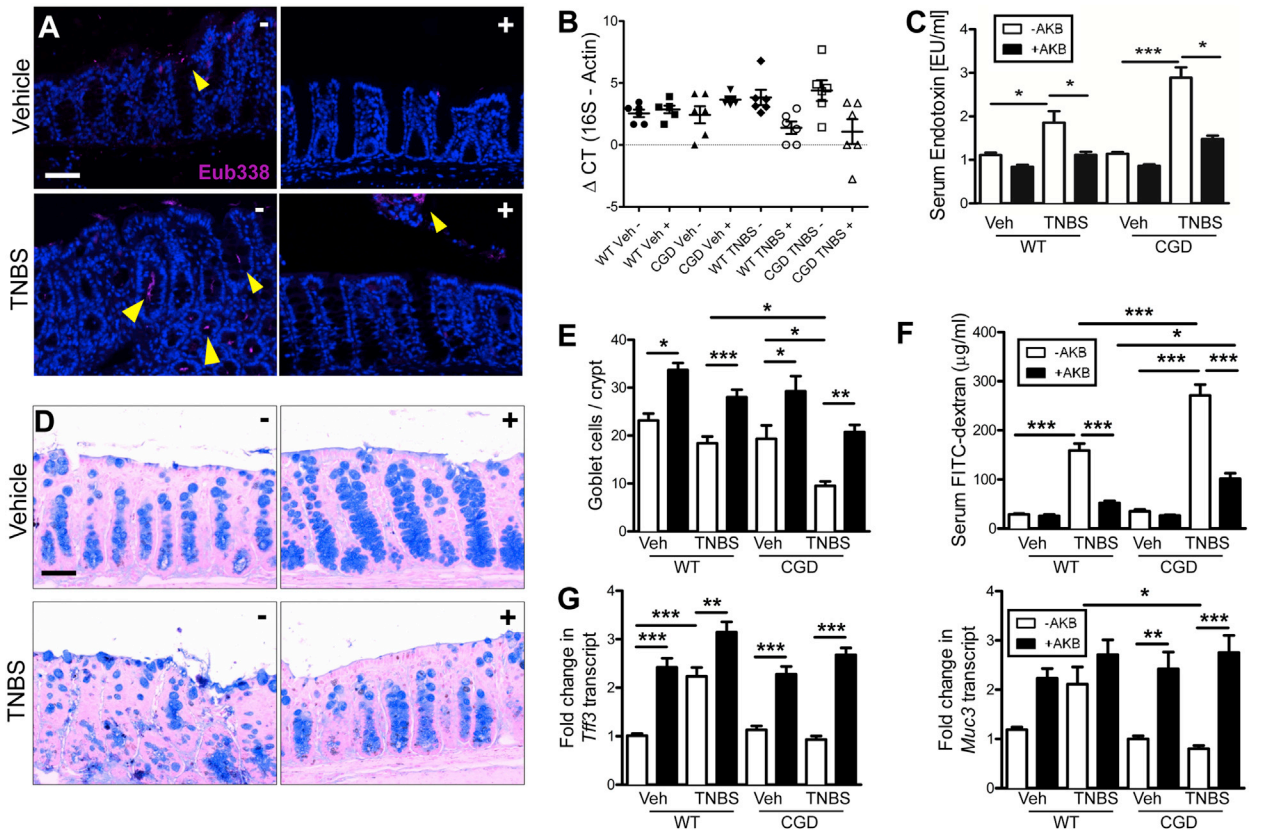

Figure 7. HIF Stabilization Promotes Mucosal Protection against Luminal Bacteria in CGD Mice via Goblet Cell Function

CGD mice treated with AKB-4924 or vehicle on days −1 through 2 and TNBS or vehicle was administered on day 0. Fluorescent in situ hybridization (FISH) was performed with Eub338 probe (magenta) in CGD mice.

(A) Representative images indicated crypt infiltration of bacteria during colitis.

(B) Quantification of bacterial dissemination to mesenteric lymph nodes was achieved by 16S rDNA qPCR. Data are presented as means ± SEM (n = 6).

(C) Serum LPS quantification was measured by LAL assay. Data are represented as means ± SEM of three pooled experiments (n = 8–12).

(D) Representative Alcian blue staining staining for goblet cells from CGD mice.

(E) Quantification of goblet cell number per crypt in CGD mice.

(F) GI permeability was assessed by measuring serum FITC 4 hr after gavage. Data are represented as mean ± SEM of three pooled experiments (n = 8–12).

(G) Real-time qPCR of mucosal epithelial hypoxia target genes involved in regulating mucus barrier *Tff3* and *Muc3*. Data are represented as means ± SEM of three pooled experiments (n = 8–12).

*p < 0.05; **p < 0.01; ***p < 0.001; one-way ANOVA. See also Figure 7.

blood by cardiac puncture. Bacterial dissemination was quantified by qPCR for 16S rDNA in MLN (Figure 7B) and serum LPS measurements (Figure 7C), both indicating an increased bacterial load in CGD mice after TNBS treatment, prevented by pretreatment with AKB-4924.

To investigate whether the decreased bacterial infiltration was mitigated via altered epithelial barrier function, we examined mucus production by Alcian blue staining in CGD (Figure 7D) and wild-type (Figure S7B) mice. More intense staining of goblet cells were observed and quantification of goblet cell numbers per crypt (Figure 7E) revealed an increase after PHD inhibition. Concordantly, epithelial barrier permeability was determined by assaying serum fluorescence after FITC-dextran gavage (Figure 7F). We conducted qPCR from enriched epithelial isolates for known HIF-dependent barrier protective genes that modulate the mucus layer, *Muc3* (Louis et al., 2006) and *Tff3* (Furuta et al., 2001), both of which were induced by AKB-4924 PHD inhibition (Figure 7G). Such results implicate a prominent induction of mucin and mucin-binding elements by PHD inhibition.

DISCUSSION

"Inflammatory hypoxia" (Karhausen et al., 2004) is thought to result from numerous factors including increased metabolic demand and decreased O_2 delivery (Colgan and Taylor, 2010). Here, we demonstrate that actively migrating PMNs establish a microenvironment permitting surrounding tissues to "sense" O_2 depletion. Epithelial cells left in the wake of migrating PMNs become transcriptionally imprinted, displaying a prominent hypoxic signature. By utilizing both a "direct" and "indirect" transmigration model and examining genes regulated similarly in both, we were able to exclude the potential for PMN gene contamination. Our in vitro real-time oxygen-sensing experiments demonstrate the extent of oxygen depletion in media after

PMN activation, despite continuous mixing. Incubation of epithelia with indirect supernatants also resulted in HIF stabilization, which we attributed simply to oxygen depletion. Although we cannot outright exclude other mechanisms, for instance epithelial-derived exosomes (Bobrie et al., 2012), PMN-derived microparticles (Dalli and Serhan, 2012; Lim et al., 2013) effecting intercellular genetic communication via microRNAs (Mittelbrunn and Sánchez-Madrid, 2012), or adenosine-mediated non-oxygen-related signaling pathways such as deneddylation of Cul-2-containing RING ligases (Ehrentraut et al., 2013) leading to HIF-1α stabilization in normal oxygen tensions, ultimately the endpoint is epithelial HIF signaling.

Given the protective nature of HIF in the mucosa, such findings reveal a previously unappreciated molecular mechanism for PMN-mediated resolution of inflammation. Likewise, NF-κB has been demonstrated to be antiapoptotic in intestinal epithelia and is protective in murine models of colitis (Chen et al., 2003). The stabilization and activity of both NF-κB and HIFα subunits are regulated by the O_2-dependent PHDs (prolyl hydroxylases). Inhibition of PHDs results in enhanced HIF and NF-κB activity and has been implicated as mucosal protective in both DSS (Cummins et al., 2008) and TNBS (Robinson et al., 2008) models of colitis.

ODD-luciferase mice permitted quantification of inflammatory hypoxia in experimental colitis. Consistent with previous work (Karhausen et al., 2004), this analysis revealed prominent stabilization of HIF in both the cecum and in patchy regions along the wall of the colonic mucosa. Patient samples mirrored this finding, revealing concomitant staining of HIF-target Glut-1 in epithelia surrounding crypt abscesses. Antibody-mediated depletion of murine PMNs indicated that PMNs fundamentally contribute to the establishment of the hypoxic microenvironment evident during acute inflammation. Consistent with previous work in rats (Kühl et al., 2007), PMN depletion exacerbated colitis, suggesting that stabilization of HIF, by infiltrating PMNs in the present work, promotes a protective phenotype within the mucosa.

Mechanistically, PMN-mediated tissue hypoxia required a functional respiratory burst, mediated via the PMN NADPH oxidase complex (Nauseef, 2008). Use of the flavoprotein inhibitor DPI and CGD mice implicated NADPH oxidase in O_2 depletion and stabilization of HIF in adjacent epithelia. Murine CGD PMNs were incapable of generating a hypoxic microenvironment or stabilizing epithelial HIF. Of interest in this regard, it is recognized that a subset of CGD patients develop colonic inflammation (Huang et al., 2004). Consistent with this clinical observation, CGD mice developed a severe colitic phenotype. Although the epithelium remained relatively intact in wild-type mice with TNBS, severe damage to the mucosa occurred, accompanied by a lack of discernible pimonidazole adduct localization in CGD mice and a greater influx of PMNs. Likewise, our results demonstrated that HIF stabilizers (PHD inhibitors) are sufficient to provide mucosal protection and abrogate the CGD phenotype.

Neutrophil numbers decrease during resolution of TNBS colitis as a result of clearance by macrophages (Cox et al., 1995; Savill et al., 1989). In the CGD mice, neutrophil and macrophage numbers are increased in the absence of a respiratory burst, potentially indicative of failed clearance (Sanmun et al., 2009). PHD inhibition was protective against the CGD colitis phenotype, restoring PMN and monocyte levels to normal, concomitant with enhanced tissue protection and mucosal HIF stabilization. Whereas the PHD inhibitor AKB-4924 has been recently demonstrated to augment the antimicrobial activity of PMNs independent of the respiratory burst (Okumura et al., 2012), our studies demonstrate diminished bacterial translocation as a result of enhanced mucosal barrier function, which probably has a greater impact in the CGD mice. Identification of bacteria deep in the colonic crypts of CGD mice after colitis, coupled with aberrant goblet cell distribution throughout the crypts that was reversible with PHD inhibition, suggested that AKB-4924 may influence goblet cell survival or function. Adherent and fluid mucus layers, secreted by goblet cells, limit physical interaction with luminal bacteria (Johansson et al., 2011). Impaired goblet cell function or mucus layer forming proteins (Muc2, Tff3) have been implicated in the pathogenesis of chronic colonic inflammation (Beck et al., 2010; Van der Sluis et al., 2006). We examined murine epithelial *Muc3* and *Tff3*, known HIF-dependent gene products, as a proof-of-principle and demonstration that colonic mucus was being affected. HIF has been implicated in goblet cell hyperplasia in the lung (Polosukhin et al., 2011). Moreover, *Tff3* expression has been implicated in limiting epithelial apoptosis (Taupin et al., 2000) and promoting mucosal healing (Mashimo et al., 1996), possibly via induction of IL-6 (Taupin and Podolsky, 2003). Considering the sheer plethora of potential innate and adaptive deficiencies potentially associated with chronic inflammatory conditions like ulcerative colitis (Khor et al., 2011), it is unclear whether PHD inhibition could provide a viable therapeutic option. However, as mentioned previously, the innate deficit in CGD patients often leads to severe chronic colonic inflammation similar to ulcerative colitis (Huang et al., 2004).

Taken together, these results provide molecular insight into the role of PMNs in inflammatory resolution. Transcriptional imprinting of select signaling pathways, exemplified here by HIF, provides mucosal memory after the clearance of PMNs and elicits functional resolution responses important to tissue homeostasis. Although PMN accumulation in crypt abscesses is a hallmark of mucosal inflammation, our findings suggest that PMN infiltration is a necessity for limiting disease severity. Our studies show that the respiratory burst is fundamental for initiating a hypoxic microenvironment, impeding further PMN infiltration, and that restoring hypoxic signaling to the mucosa is sufficient to overcome the resolution deficit (e.g., in CGD mice). These findings demonstrate the beneficial impact and regulatory influence of PMN-mediated HIF stabilization within discrete regions of the mucosa and provide important insight into therapeutic options for inflammatory mucosal disease.

EXPERIMENTAL PROCEDURES

Materials and Methods

IECs were cultured and transfected as described previously (Campbell et al., 2010). Caco-2 were used for transfections; T84 were used for all other in vitro experiments. HIF-1α and tissue cytokines were quantified by Mesoscale (MSD). PHD inhibitor (AKB-4924) was provided by Akebia Pharmaceuticals.

Neutrophil-Epithelial Interaction Models

Neutrophils were subjected to either direct transmigration, indirect transmigration, coculture, or SDR real-time O_2 models (Figure S1). For direct

transmigration, T84 IECs were grown to confluence (TER > 2,000 $\Omega \cdot cm^2$) on the underside of collagen-coated Transwell 5.0 μm pore permeable supports (Corning). A chemotactic agent (1 μM fMLF in HBSS) was applied to the apical surface (bottom chamber). Neutrophils (1×10^6) were applied to the basolateral side (top) to allow transmigration in the physiologically relevant basolateral-apical direction. In the indirect model, conditioned supernatants from direct transmigration were collected, clarified by centrifugation (350 × *g* for 10 min), and applied to naive T84 monolayers. In the coculture model, epithelial cells were cultured in 24-well plates. PMNs were suspended above them on permeable supports that prevented physical interaction between PMNs and epithelia (0.4 μm pore).

O_2 Measurements

Initial pO_2 experiments were carried out with an Oxylite 2000 probe (Oxford Optronix). Measurements were performed at 4% O_2 in a hypoxia chamber. Subsequent real-time O_2 measurements were made with Oxodish plates on an SDR reader (PreSens) and performed in normoxia. Oxodish 24-well plates were pre-equilibrated with HBSS+ or HBSS+ containing either fMLF or PMA. Transwell filters (Corning; 0.4 μm pore) were suspended above the O_2 sensor to physically separate PMNs from the sensor. Freshly isolated neutrophils from either whole venous blood of healthy volunteers or mouse bone-marrow-derived PMNs were applied to the filter.

Microarray and Analysis

Cyanine-3 (Cy3)-labeled cRNA was prepared from 0.2 μg total RNA via the One-Color Quick Amp Labeling kit (Agilent) according to the manufacturer's instructions, followed by RNAeasy column purification (QIAGEN). Cy3-labeled cRNA and hybridized to Agilent 4x44K human whole-genome arrays. Data were analyzed with GeneSpring GX12 (Agilent Technologies).

Patient Samples and Histological Scoring

Sections from archived biopsy tissue from IBD patients were obtained according to approved human research protocols from the Colorado Multi-Institutional Review Board and screened for presence of active disease with crypt abscesses. Histological assessment was performed by a pathologist (P.J.), blinded to strain and treatment groups. The following standardized semiquantitative system scores were applied for the following parameters: (1) active inflammation (granulocyte infiltration); (2) chronic inflammation (lymphocytes and macrophages in the mucosa and submucosa); and (3) colonic gland distortion. Biopsy samples with crypt abscesses were used for immunohistochemical analysis.

Mice and Chemically Induced Colitis

Wild-type (C57BL/6), CGD (*Nox2*$^{-/-}$), and ODD-luciferase mice were purchased from Jackson Laboratories. Mice were housed in ventilated cages. One week prior to induction of colitis, mice were presensitized by skin painting with 1% TNBS in 80% EtOH. On day 0, mice were anesthetized and received a 100 μl rectal instillation of either vehicle (50% EtOH) or TNBS (2.5% TNBS in 50% EtOH). For neutrophil depletion, mice were injected with either 1 mg/kg i.p. of Gr-1 or sham (isotype control rat IgG2b), on days −1 and day 0, prior to TNBS rectal instillation. Daily treatment with 5 mg/kg either AKB-4924 or vehicle (carboxymethylcellulose) by i.p. injection occurred on days −1 through day 2. Colons were removed from ODD-luciferase mice after TNBS administration for bioluminescent imaging with an IVIS Imaging System 50 Series (Caliper Life Sciences/Xenogen Corp). Animal protocols were approved by the Institutional Animal Care and Use Committee at the University of Colorado.

Epithelial Enrichment, Immune Cell Isolation, and Flow Cytometry

For demonstration of granulocyte depletion, whole blood was collected from anesthetized animals by cardiac puncture and anticoagulated with K2-EDTA.

Mouse colonic sections were prepared by removal of the epithelium in HBSS- with 5 mM EDTA. After agitation, liberated epithelia were removed by passing through a 70 μm pore filter. Remaining tissue was digested for immune cell isolation. Flow-through epithelia were washed in HBSS- and purified by immunomagnetic negative selection with the EasySep Mouse epithelial cell enrichment kit (StemCell Technologies) as directed by manufacturer. Recovered epithelia were immediately processed for RNA isolation.

Remaining tissue was digested at 37°C for 15 min with agitation in digestion buffer (1 mg/ml Collagenase [Sigma], 0.5 mg/ml Dispase [GIBCO], 0.1 mg/ml DNase I [Sigma] in RPMI 1640 [HyClone] with 1% FBS [GIBCO]) and subsequently neutralized with an equal volume of cold complete medium. Debris was removed by decanting through 70 μm pore mesh filter. Cells were pelleted and resuspended in FACS buffer (5% FBS, 1% BSA, 0.1% NaN_3 in PBS).

Cells were incubated with fluorescently labeled antibodies against mouse CD45 (30-F11) MHC class II (M5/114.15.2), CD11c (N418), Ly6c (HK1.4) (eBioscience), CD11b (M1/70), Ly6g (1A8), and SiglecF (E50-2440) (BD Bioscience), or corresponding isotype controls. Cells were fixed with 2% paraformaldehyde and 7-color analysis was performed with a BD FACSCanto II (BD Biosciences). Data were analyzed with BD FACS Diva software (BD Biosciences).

ACCESSION NUMBERS

The microarray data are available in the Gene Expression Omnibus (GEO) database (http://www.ncbi.nlm.nih.gov/gds) under the accession number GSE39681.

SUPPLEMENTAL INFORMATION

Supplemental Information includes Supplemental Experimental Procedures and seven figures and can be found with this article online at http://dx.doi.org/10.1016/j.immuni.2013.11.020.

ACKNOWLEDGMENTS

We thank R. Reisdorph for technical assistance and C. Wilson and E. Lee for procurement of tissues for histological analysis. Work was supported by NIH grants DK050189, DK095491, HL60569, and DK088663 and by a CCFA Career Development Award (to E.L.C.).

Received: December 5, 2012
Accepted: November 8, 2013
Published: January 9, 2014

REFERENCES

Amulic, B., Cazalet, C., Hayes, G.L., Metzler, K.D., and Zychlinsky, A. (2012). Neutrophil function: from mechanisms to disease. Annu. Rev. Immunol. *30*, 459–489.

Beck, P.L., Ihara, E., Hirota, S.A., MacDonald, J.A., Meng, D., Nanthakumar, N.N., Podolsky, D.K., and Xavier, R.J. (2010). Exploring the interplay of barrier function and leukocyte recruitment in intestinal inflammation by targeting fucosyltransferase VII and trefoil factor 3. Am. J. Physiol. Gastrointest. Liver Physiol. *299*, G43–G53.

Bobrie, A., Krumeich, S., Reyal, F., Recchi, C., Moita, L.F., Seabra, M.C., Ostrowski, M., and Théry, C. (2012). Rab27a supports exosome-dependent and -independent mechanisms that modify the tumor microenvironment and can promote tumor progression. Cancer Res. *72*, 4920–4930.

Brinkmann, V., Reichard, U., Goosmann, C., Fauler, B., Uhlemann, Y., Weiss, D.S., Weinrauch, Y., and Zychlinsky, A. (2004). Neutrophil extracellular traps kill bacteria. Science *303*, 1532–1535.

Campbell, E.L., MacManus, C.F., Kominsky, D.J., Keely, S., Glover, L.E., Bowers, B.E., Scully, M., Bruyninckx, W.J., and Colgan, S.P. (2010). Resolvin E1-induced intestinal alkaline phosphatase promotes resolution of inflammation through LPS detoxification. Proc. Natl. Acad. Sci. USA *107*, 14298–14303.

Chen, L.W., Egan, L., Li, Z.W., Greten, F.R., Kagnoff, M.F., and Karin, M. (2003). The two faces of IKK and NF-kappaB inhibition: prevention of systemic inflammation but increased local injury following intestinal ischemia-reperfusion. Nat. Med. *9*, 575–581.

Colgan, S.P., and Taylor, C.T. (2010). Hypoxia: an alarm signal during intestinal inflammation. Nat Rev Gastroenterol Hepatol *7*, 281–287.

Colgan, S.P., Curtis, V.F., and Campbell, E.L. (2013a). The inflammatory tissue microenvironment in IBD. Inflamm. Bowel Dis. *19*, 2238–2244.

Colgan, S.P., Ehrentraut, S.F., Glover, L.E., Kominsky, D.J., and Campbell, E.L. (2013b). Contributions of neutrophils to resolution of mucosal inflammation. Immunol. Res. *55*, 75–82.

Cox, G., Crossley, J., and Xing, Z. (1995). Macrophage engulfment of apoptotic neutrophils contributes to the resolution of acute pulmonary inflammation in vivo. Am. J. Respir. Cell Mol. Biol. *12*, 232–237.

Cross, A.R., and Jones, O.T. (1986). The effect of the inhibitor diphenylene iodonium on the superoxide-generating system of neutrophils. Specific labelling of a component polypeptide of the oxidase. Biochem. J. *237*, 111–116.

Cross, A.R., and Segal, A.W. (2004). The NADPH oxidase of professional phagocytes—prototype of the NOX electron transport chain systems. Biochim. Biophys. Acta *1657*, 1–22.

Cummins, E.P., Seeballuck, F., Keely, S.J., Mangan, N.E., Callanan, J.J., Fallon, P.G., and Taylor, C.T. (2008). The hydroxylase inhibitor dimethyloxalylglycine is protective in a murine model of colitis. Gastroenterology *134*, 156–165.

Dalli, J., and Serhan, C.N. (2012). Specific lipid mediator signatures of human phagocytes: microparticles stimulate macrophage efferocytosis and pro-resolving mediators. Blood *120*, e60–e72.

Dinauer, M.C., Orkin, S.H., Brown, R., Jesaitis, A.J., and Parkos, C.A. (1987). The glycoprotein encoded by the X-linked chronic granulomatous disease locus is a component of the neutrophil cytochrome b complex. Nature *327*, 717–720.

Ehrentraut, S.F., Kominsky, D.J., Glover, L.E., Campbell, E.L., Kelly, C.J., Bowers, B.E., Bayless, A.J., and Colgan, S.P. (2013). Central role for endothelial human deneddylase-1/SENP8 in fine-tuning the vascular inflammatory response. J. Immunol. *190*, 392–400.

Furuta, G.T., Turner, J.R., Taylor, C.T., Hershberg, R.M., Comerford, K., Narravula, S., Podolsky, D.K., and Colgan, S.P. (2001). Hypoxia-inducible factor 1-dependent induction of intestinal trefoil factor protects barrier function during hypoxia. J. Exp. Med. *193*, 1027–1034.

Huang, J.S., Noack, D., Rae, J., Ellis, B.A., Newbury, R., Pong, A.L., Lavine, J.E., Curnutte, J.T., and Bastian, J. (2004). Chronic granulomatous disease caused by a deficiency in p47(phox) mimicking Crohn's disease. Clin. Gastroenterol. Hepatol. *2*, 690–695.

Johansson, M.E., Larsson, J.M., and Hansson, G.C. (2011). The two mucus layers of colon are organized by the MUC2 mucin, whereas the outer layer is a legislator of host-microbial interactions. Proc. Natl. Acad. Sci. USA *108* (*Suppl 1*), 4659–4665.

Karhausen, J., Furuta, G.T., Tomaszewski, J.E., Johnson, R.S., Colgan, S.P., and Haase, V.H. (2004). Epithelial hypoxia-inducible factor-1 is protective in murine experimental colitis. J. Clin. Invest. *114*, 1098–1106.

Khor, B., Gardet, A., and Xavier, R.J. (2011). Genetics and pathogenesis of inflammatory bowel disease. Nature *474*, 307–317.

Kominsky, D.J., Campbell, E.L., and Colgan, S.P. (2010). Metabolic shifts in immunity and inflammation. J. Immunol. *184*, 4062–4068.

Kühl, A.A., Kakirman, H., Janotta, M., Dreher, S., Cremer, P., Pawlowski, N.N., Loddenkemper, C., Heimesaat, M.M., Grollich, K., Zeitz, M., et al. (2007). Aggravation of different types of experimental colitis by depletion or adhesion blockade of neutrophils. Gastroenterology *133*, 1882–1892.

Lim, K., Sumagin, R., and Hyun, Y.M. (2013). Extravasating neutrophil-derived microparticles preserve vascular barrier function in inflamed tissue. Immune Netw. *13*, 102–106.

Louis, N.A., Hamilton, K.E., Canny, G., Shekels, L.L., Ho, S.B., and Colgan, S.P. (2006). Selective induction of mucin-3 by hypoxia in intestinal epithelia. J. Cell. Biochem. *99*, 1616–1627.

Mashimo, H., Wu, D.C., Podolsky, D.K., and Fishman, M.C. (1996). Impaired defense of intestinal mucosa in mice lacking intestinal trefoil factor. Science *274*, 262–265.

Mittelbrunn, M., and Sánchez-Madrid, F. (2012). Intercellular communication: diverse structures for exchange of genetic information. Nat. Rev. Mol. Cell Biol. *13*, 328–335.

Nauseef, W.M. (2008). Biological roles for the NOX family NADPH oxidases. J. Biol. Chem. *283*, 16961–16965.

Okumura, C.Y., Hollands, A., Tran, D.N., Olson, J., Dahesh, S., von Köckritz-Blickwede, M., Thienphrapa, W., Corle, C., Jeung, S.N., Kotsakis, A., et al. (2012). A new pharmacological agent (AKB-4924) stabilizes hypoxia inducible factor-1 (HIF-1) and increases skin innate defenses against bacterial infection. J. Mol. Med. *90*, 1079–1089.

Polosukhin, V.V., Cates, J.M., Lawson, W.E., Milstone, A.P., Matafonov, A.G., Massion, P.P., Lee, J.W., Randell, S.H., and Blackwell, T.S. (2011). Hypoxia-inducible factor-1 signalling promotes goblet cell hyperplasia in airway epithelium. J. Pathol. *224*, 203–211.

Radi, R., Beckman, J.S., Bush, K.M., and Freeman, B.A. (1991). Peroxynitrite oxidation of sulfhydryls. The cytotoxic potential of superoxide and nitric oxide. J. Biol. Chem. *266*, 4244–4250.

Robinson, A., Keely, S., Karhausen, J., Gerich, M.E., Furuta, G.T., and Colgan, S.P. (2008). Mucosal protection by hypoxia-inducible factor prolyl hydroxylase inhibition. Gastroenterology *134*, 145–155.

Safran, M., Kim, W.Y., O'Connell, F., Flippin, L., Günzler, V., Horner, J.W., Depinho, R.A., and Kaelin, W.G., Jr. (2006). Mouse model for noninvasive imaging of HIF prolyl hydroxylase activity: assessment of an oral agent that stimulates erythropoietin production. Proc. Natl. Acad. Sci. USA *103*, 105–110.

Sanmun, D., Witasp, E., Jitkaew, S., Tyurina, Y.Y., Kagan, V.E., Ahlin, A., Palmblad, J., and Fadeel, B. (2009). Involvement of a functional NADPH oxidase in neutrophils and macrophages during programmed cell clearance: implications for chronic granulomatous disease. Am. J. Physiol. Cell Physiol. *297*, C621–C631.

Savill, J.S., Wyllie, A.H., Henson, J.E., Walport, M.J., Henson, P.M., and Haslett, C. (1989). Macrophage phagocytosis of aging neutrophils in inflammation. Programmed cell death in the neutrophil leads to its recognition by macrophages. J. Clin. Invest. *83*, 865–875.

Serhan, C.N., and Chiang, N. (2013). Resolution phase lipid mediators of inflammation: agonists of resolution. Curr. Opin. Pharmacol. *13*, 632–640.

Stie, J., and Jesaitis, A.J. (2007). Reorganization of the human neutrophil plasma membrane is associated with functional priming: implications for neutrophil preparations. J. Leukoc. Biol. *81*, 672–685.

Taupin, D., and Podolsky, D.K. (2003). Trefoil factors: initiators of mucosal healing. Nat. Rev. Mol. Cell Biol. *4*, 721–732.

Taupin, D.R., Kinoshita, K., and Podolsky, D.K. (2000). Intestinal trefoil factor confers colonic epithelial resistance to apoptosis. Proc. Natl. Acad. Sci. USA *97*, 799–804.

Van der Sluis, M., De Koning, B.A., De Bruijn, A.C., Velcich, A., Meijerink, J.P., Van Goudoever, J.B., Büller, H.A., Dekker, J., Van Seuningen, I., Renes, I.B., and Einerhand, A.W. (2006). Muc2-deficient mice spontaneously develop colitis, indicating that MUC2 is critical for colonic protection. Gastroenterology *131*, 117–129.

Van Rees, E.P., Palmen, M.J., Van De Goot, F.R., Macher, B.A., and Dieleman, L.A. (1997). Leukocyte migration in experimental inflammatory bowel disease. Mediators Inflamm. *6*, 85–93.

Zen, K., and Parkos, C.A. (2003). Leukocyte-epithelial interactions. Curr. Opin. Cell Biol. *15*, 557–564.